$CO_2$ Electroreduction Hot Paper

International Edition: DOI: 10.1002/anie.201704613
German Edition: DOI: 10.1002/ange.201704613

# Enhanced Carbon Dioxide Electroreduction to Carbon Monoxide over Defect-Rich Plasma-Activated Silver Catalysts

*Hemma Mistry, Yong-Wook Choi, Alexander Bagger, Fabian Scholten, Cecile S. Bonifacio, Ilya Sinev, Nuria J. Divins, Ioannis Zegkinoglou, Hyo Sang Jeon, Kim Kisslinger, Eric A. Stach, Judith C. Yang, Jan Rossmeisl,* and Beatriz Roldan Cuenya**

***Abstract:*** *Efficient, stable catalysts with high selectivity for a single product are essential if electroreduction of $CO_2$ is to become a viable route to the synthesis of industrial feedstocks and fuels. A plasma oxidation pre-treatment of silver foil enhances the number of low-coordinated catalytically active sites, which dramatically lowers the overpotential and increases the activity of $CO_2$ electroreduction to CO. At −0.6 V versus RHE more than 90% Faradaic efficiency towards CO was achieved on a pre-oxidized silver foil. While transmission electron microscopy (TEM) and operando X-ray absorption spectroscopy showed that oxygen species can survive in the bulk of the catalyst during the reaction, quasi in situ X-ray photoelectron spectroscopy showed that the surface is metallic under reaction conditions. DFT calculations reveal that the defect-rich surface of the plasma-oxidized silver foils in the presence of local electric fields drastically decrease the overpotential of $CO_2$ electroreduction.*

The electroreduction of $CO_2$ is a promising technology that could provide a means to synthesize alternative hydrocarbon fuels by consuming waste emissions.[1] However, efficient, stable, and inexpensive catalysts are still needed to electrochemically reduce $CO_2$ while suppressing the $H_2$ evolution (HER) side reaction. While gold catalysts show high activity and selectivity to CO at moderate overpotentials,[2] silver (Ag) is considerably cheaper, and it can also achieve near to 100% selectivity towards CO at higher overpotential.[3] Nanostructuring the surface is one method which may improve the reactivity of Ag-based catalysts for $CO_2$ electroreduction.[4] For example, nanoporous Ag has been shown to have improved performance in comparison to flat Ag,[4a,5] possibly because of the enhanced binding of intermediates at low-coordinated atomic sites[6] or to mesoscale transport effects.[5b] Ag nanoparticles have also shown increased activity for $CO_2$ reduction to CO with decreasing particle size down to 5 nm.[4b,c] Recent attention has also been paid to metal catalysts (including Ag[7]) that are pre-oxidized and then reduced in situ under $CO_2$ electroreduction conditions; vastly improved reactivity was observed in comparison to unoxidized catalysts.[8] However, the mechanism causing their improved behavior is under debate. A consistent picture is still required that describes the role of subsurface oxygen and cationic metal species versus morphological surface modifications (roughening and nanostructuring) for Ag catalysts.

Herein, we used plasma treatments to synthesize oxidized and highly defective nanostructured Ag catalysts for selective $CO_2$ electroreduction to CO at low overpotential. Advanced in situ and operando X-ray spectroscopy measurements showed that while oxygen could survive in the bulk of the catalyst during the reaction, the near-surface region of the catalyst is metallic. Using density functional theory (DFT) calculations, the enhanced activity could be assigned to the highly under-coordinated surface of the pre-oxidized catalysts, which can lower the overpotential for $CO_2$ reduction in the presence of local electric fields.

Nanostructured Ag catalysts were synthesized by treating Ag foils in low-pressure plasmas of $H_2$, Ar, or $O_2$ gas. Figure 1 and Figure S1 (Supporting Information) show scanning electron microscopy (SEM) images of Ag catalysts after surface structuring with the plasma treatments. Ar or $H_2$ plasma introduces small, pore-like defects 50–100 nm in size onto the surface, while $O_2$ plasma causes significant roughening and dense, approximately 50 nm large pores on the Ag foil. $O_2$ plasma followed by a further $H_2$ plasma treatment ($O_2 + H_2$ sample) results in further nanostructuring of the Ag surface. The bottom row of Figure 1 shows the samples after 1 h of $CO_2$ electroreduction at −0.6 V versus RHE. While only mild changes are apparent in the Ar-treated sample, the $O_2$-treated samples show a drastic increase in surface roughness after the reaction, particularly for the $O_2 + H_2$ sample. These changes may be related to the rapid growth of Ag

[*] Dr. H. Mistry, Y.-W. Choi, F. Scholten, Dr. I. Sinev, Dr. N. J. Divins, Dr. I. Zegkinoglou, Dr. H. S. Jeon, Prof. B. Roldan Cuenya
Department of Physics, Ruhr University Bochum
44780 Bochum (Germany)
E-mail: Beatriz.Roldan@rub.de

Dr. H. Mistry
Department of Physics, University of Central Florida
Orlando, FL 32816 (USA)

A. Bagger, Prof. J. Rossmeisl
Department of Chemistry, University of Copenhagen
Copenhagen (Denmark)
E-mail: jan.rossmeisl@chem.ku.dk

Dr. C. S. Bonifacio, Prof. J. C. Yang
Chemical and Petroleum Engineering and Physics
University of Pittsburgh
Pittsburgh, PA 15261 (USA)

K. Kisslinger, Dr. E. A. Stach
Center for Functional Nanomaterials
Brookhaven National Laboratory
Upton, New York 11973 (USA)

Prof. B. Roldan Cuenya
Department of Interface Science, Fritz-Haber Institute of the Max Planck Society, 14195 Berlin (Germany)

Supporting information and the ORCID identification number(s) for the author(s) of this article can be found under: https://doi.org/10.1002/anie.201704613.

  

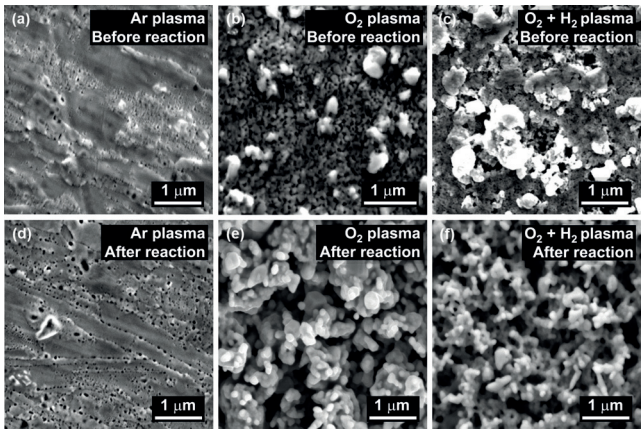


***Figure 1.*** SEM images of plasma-treated Ag foils a–c) as prepared and d–f) after 1 h of $CO_2$ electroreduction at −0.6 V vs. RHE.

oxides during $O_2$ plasma and their subsequent reduction under reaction conditions. SEM measurements of the pre-oxidized catalysts measured after longer reaction times (3 h) show that the surface structure continues to change over time (Supporting Information, Figure S2).

Cross-sections of several of the samples were prepared, and scanning transmission electron microscopy—energy dispersive X-ray spectroscopy (STEM-EDS) was measured before and after the reaction to gain further insight into the nanostructuring and the changes in oxidation state of the catalysts caused by the plasma treatments. Figures 2 a and 2 b show the Ar plasma-treated sample before reaction. Ar plasma causes pore formation not only on the surface but also below. This pore formation is a result of the plasma treatment, and not an artifact from the sample preparation, as proved by comparison with an untreated Ag sample that shows no pore formation (Supporting Information, Figure S3). For the Ar plasma-treated sample, the EDS results also indicate only 1 atomic weight % of O in the top 500 nm of the surface. After the reaction, Figure 2 c shows that no major changes occurred to the structure and oxide content of the Ar plasma sample. In comparison, the $O_2$ plasma-treated Ag foil before reaction is very rough and porous and has a high oxygen content (compare to Figures 2 d—f). A 35–50 nm thick layer of AgO exists on the surface, while below the surface Ag grains and regions with about 20 % O atom content are present. After 1 h of reaction, the porosity increases, the surface oxide layer has lower oxygen content, and oxygen remains in the bulk of the sample (ca. 6 % O). The SEM and STEM images before and after reaction were not measured at identical locations, and so it must be considered that heterogeneities in the sample may in part explain some of the differences before and after reaction. However, we measured several regions within each sample under the different conditions by SEM and we observed similar structures. Our results indicate that plasma treatment with atomic oxygen can heavily oxidize, roughen, and create defects on an Ag surface, and oxygen can remain in the bulk of these catalysts under the reducing conditions of $CO_2$ electroreduction.

To resolve changes in the structure and oxidation state of these catalysts under reaction conditions, we measured extended X-ray absorption fine structure (EXAFS) on the plasma-treated Ag catalysts during $CO_2$ electroreduction. The measurements were performed at a small incidence angle to increase the surface sensitivity. In their initial state, the Ar and $H_2$ plasma-treated foils appear similar in EXAFS to an untreated Ag foil (that is, in their metallic state; Supporting Information, Figure S4 and Table S1), while the $O_2$ and $O_2 + H_2$-treated samples showed Ag–Ag coordination numbers below 7 and the presence of Ag–O bonds (Figure 3; Supporting Information, Table S2). The $O_2$ and the $O_2 + H_2$ plasma samples were measured in operando during $CO_2$ electroreduction for 1 h at −0.6 V versus RHE in 0.1 M $KHCO_3$ (Figure 3). Impedance measurements were performed to ensure similar electrochemical conditions during operando measurements as during the lab-based measurements in the standard H-type cell (Supporting Information, Figures S5, S6, and Table S3). During the reaction, the EXAFS results show the reduction of the samples over time. For the $O_2$ plasma sample, oxides can be detected up to 30 min, and the Ag–Ag coordination number increases to 11 after 65 min of reaction. A coordination number lower than 12 may stem from the extreme roughness and porosity of the sample, or from traces of cationic Ag remaining in the sample that could not be fitted in the bulk-sensitive EXAFS data. In comparison, the $O_2 + H_2$ sample has a lower initial oxygen content because of the partial reduction of the sample surface with $H_2$ plasma. Additionally, the oxides in this sample reduce more quickly, and the Ag–Ag coordination number increased to 11 after the first 15 min. EXAFS of the Ar plasma-treated sample was also measured under operando $CO_2$ reduction conditions; however, Figure S7 and Table S3 (Supporting Information) show that the sample appeared similar in structure to an untreated metallic Ag foil and no changes could be detected over 30 min of reaction.

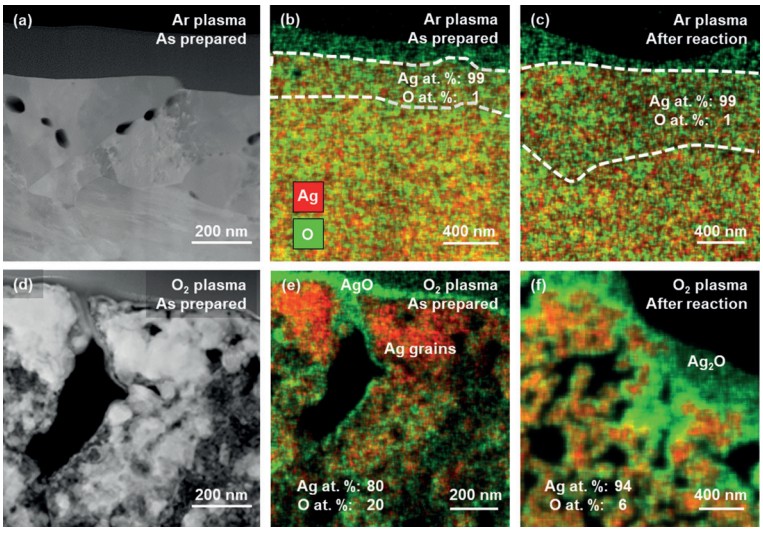


***Figure 2.*** a,d) SEM and b,c,e,f) STEM-EDS images of cross-sections of Ag foils treated with (a–c) Ar plasma and (d–f) $O_2$ plasma, before and after $CO_2$ electroreduction at −0.6 V vs. RHE.

  

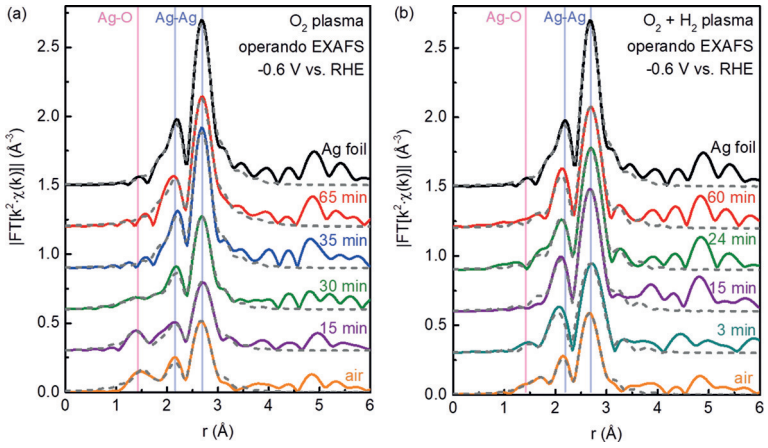


***Figure 3.*** Ag K-edge $k^2$-weighted EXAFS of a) $O_2$ plasma-treated and b) $O_2+H_2$ plasma-treated Ag foils measured in air and in operando during $CO_2$ electroreduction at −0.6 V vs. RHE; an untreated Ag foil is also plotted for comparison. Key: data (——), fitting (-----).

While the EXAFS and STEM results show the oxidation and structure of the bulk of the samples, characterizing the sample surface under reaction conditions is critical for understanding its reactivity. To probe the chemical state of the surface of the Ag catalysts during the reaction, quasi in situ X-ray photoelectron spectroscopy (XPS) measurements were performed using an electrochemical cell interfaced to an XPS system (Supporting Information, Figure S8). The $O_2$, $O_2+H_2$, and $H_2$ plasma-treated samples were measured with XPS as prepared and after 1 h of $CO_2$ electroreduction at −0.6 V versus RHE (Figures 4a and 4b). Initially, the $H_2$ sample contains metallic Ag, with an Ag $3d_{3/2}$ binding energy of 368.3 eV, while the oxidized samples are shifted to a lower binding energy of 367.5 eV, which is characteristic of Ag oxide. After reaction, the Ag 3d spectra for all three samples shows only metallic Ag. The Auger regions shown in Figure S9 (Supporting Information)

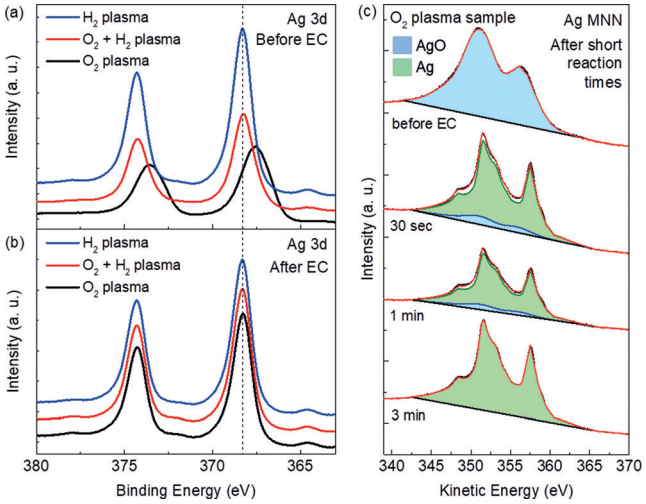


***Figure 4.*** XPS measurements of the Ag 3d region of $O_2$, $H_2$, and $O_2+H_2$ plasma-treated Ag catalysts a) as prepared and b) after 1 h of $CO_2$ electroreduction at −0.6 V vs. RHE and ultra-high vacuum (UHV) transfer to XPS. c) The Ag MNN Auger region of the $O_2$ plasma-treated sample as prepared and after short reaction times (30 s to 3 min).

support these findings. Therefore, despite the survival of oxygen species within the bulk of the sample (EXAFS), the top approximately 5 nm of the surface probed by XPS is reduced to metallic Ag after 1 h of reaction.

In addition to these measurements, XPS data (Auger MNN electron region) after short $CO_2$ electroreduction reaction times (30 s, 1 min, and 3 min at −0.6 V vs. RHE) were measured for the $O_2$ plasma-oxidized sample to gain insight into how fast the reduction of oxides occurs at the surface (Figure 4c). The Auger spectra were fitted with the line shape of Ag oxide and metallic Ag reference spectra (Ag foil oxidized for 15 min and a Ag(111) single crystal cleaned in situ, respectively). After 1 min of reaction, oxides can still be detected at the surface (ca. 9%), but not after 3 min of reaction. This is consistent with the sharp decrease in current observed when starting the reaction (Figure 5a), which corresponds to the initial reduction of Ag oxides. Therefore, it is expected that the active site of these catalysts is metallic Ag under long term operation conditions.

Figures 5a and 5b show the current density and Faradaic efficiency towards CO of the plasma-treated Ag foils during $CO_2$ electroreduction at −0.6 V versus RHE over the course of 3 h. At this potential, no $CO_2$ reduction is observed on the $H_2$ and Ar-treated foils, similar to an untreated Ag foil (Supporting Information, Figure S10). In contrast, the $O_2$ and $O_2+H_2$ plasma-treated samples show exceptional activity and more than 90% selectivity towards CO at this potential. Compared to an untreated Ag foil, the overpotential for $CO_2$ reduction on plasma-oxidized Ag has been shifted positively by about −0.5 V. Faradaic efficiency towards $H_2$ is shown in Figure S11 (Supporting Information).

The efficiency towards CO degrades slightly after 3 h of reaction on the oxidized samples because of a slight decrease in current towards CO and a growth in the HER current (Figures 5c and 5d). These time-dependent changes are likely related to the change in surface structure over the course of the reaction, as seen in the SEM images (Supporting Information, Figure S2). Electrochemical surface roughness measurements also indicate that the roughness of the surface decreases by approximately half between 1–3 h of reaction (Supporting Information, Figure S12 and Table S4). A decrease in the population of defects over time can therefore be correlated to the slow deactivation of the sample, indicating that sharp nanostructured features present earlier in the reaction may be the key surface sites that enhance $CO_2$ reduction. Notably, the Ar and $H_2$ plasma samples show higher surface roughness compared to untreated Ag (Supporting Information, Table S4), but are still unable to reduce $CO_2$ at this potential. This means that the improved reactivity of the $O_2$ plasma-treated samples is not simply due to a surface area increase, but also to the intrinsic ability of the defect sites generated on these samples to reduce $CO_2$ to CO.

To understand the effect of the oxygen plasma on the Ag samples, the reaction was studied by DFT. The reactivity is estimated by calculating the free energy differences for the

  

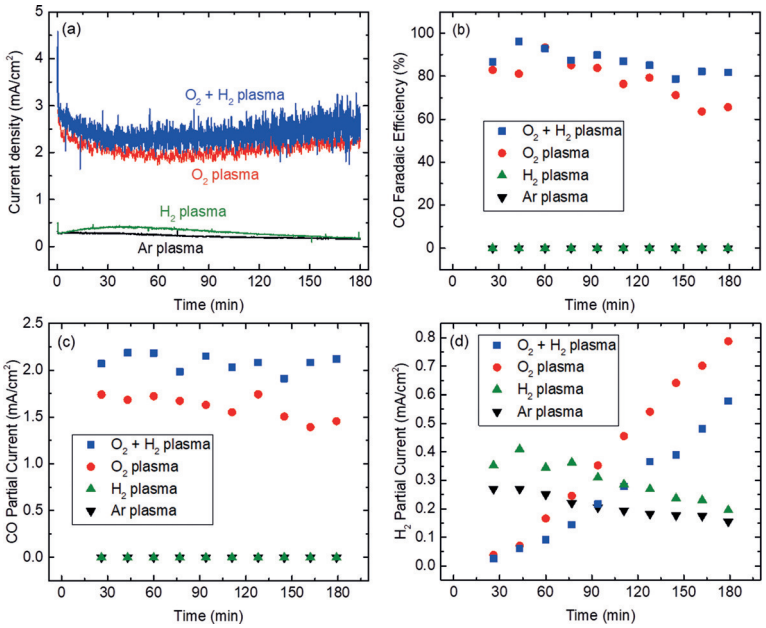


***Figure 5.*** $CO_2$ electroreduction over plasma-treated Ag foil catalysts at −0.6 V vs. RHE in 0.1 M $KHCO_3$. a) Current density, b) Faradaic efficiency towards CO, b) CO partial current, and d) $H_2$ partial current.

reduction of $CO_2$ to CO in Figure 6 as a function of the CO binding energy. The volcano-like plot is constructed from multiple models of possible Ag active sites: a 111 facet, 211 step, 111 kink, 211 and 111 adatoms, together with the Au and Cu 111 facet and 211 step. To construct the volcano-like plot, the overpotential ($-\Delta G$) was determined as the $CO_2 + H^+ + e^- \rightarrow COOH^*$ potential-dependent step on the weak-binding side, while on the strong-binding side $CO^* \rightarrow CO$ (a potential-independent step) is the reaction-limiting factor. This enabled us to create the $CO_2$ reduction volcano, where the weak- and strong-binding sides of the volcano behave differently with applied potential since they are potential dependent and independent, respectively. Thus, we display the volcano with −0.6 V (red) and with 0 V versus RHE (blue) potential applied. The potential dependence of the two sides of the volcano is also seen in the top of the volcano, which moves to the right when −0.6 V versus RHE potential is applied.

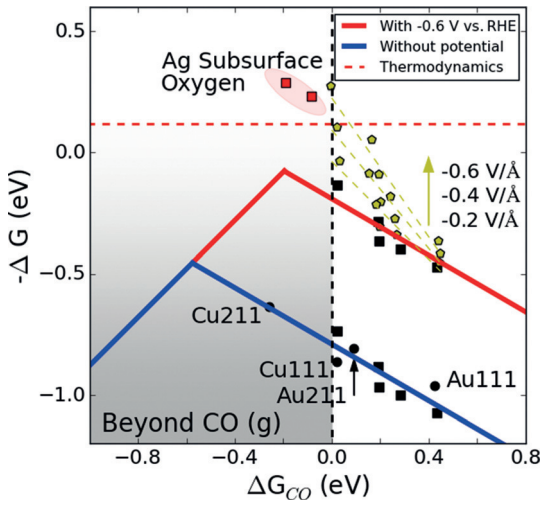


***Figure 6.*** DFT-calculated volcano plot of $CO_2$ reduction to CO; the volcano at 0 V (——) and −0.6 V (——) vs. RHE. The free energy on the weak-binding side is defined as the $CO_2 + H^+ + e^- \rightarrow COOH^*$ potential-dependent step, which is given as a function of the CO binding energy for 111 and 211 Cu and Au surfaces (●) and for multiple defective Ag surfaces (■). On the strong-binding side the potential-independent $CO^* \rightarrow CO$ step is the limiting factor. Two Ag subsurface oxygen structures have been included at −0.6 V vs. RHE potential (■). The Ag defect sites with applied negative electric field are shown in yellow.

The 111 adatom Ag defect has the lowest overpotential to reduce $CO_2$, at around −0.8 V versus RHE (for the free energy diagram see the Supporting Information, Figure S13). However, the oxygen plasma-treated Ag samples can reduce $CO_2$ at −0.6 V versus RHE. To determine if subsurface oxygen could further lower the overpotential, two structures with subsurface oxygen were investigated, labeled in Figure 6 as "Ag Subsurface Oxygen" (red squares at −0.6 V vs. RHE) and also shown in Figures S14 and S15 (for the free energy diagram see the Supporting Information) for the HER. However, as described in more detail in the Supporting Information, the results obtained from these structures deviated strongly from experimental results (for example, further reduction beyond CO or an increase in the HER was predicted but not experimentally observed), making subsurface oxygen an unlikely explanation for the low-overpotential $CO_2$ reduction.

Further investigation of the Ag defect sites shows an increased negative dipole moment for the COOH* adsorbate (Supporting Information, Figure S16), while the CO* adsorbate dipole moment is almost constant. Notably, the dipole moment for the adsorbate has been isolated by subtracting the structure dipole moment. The difference in dipole moment of these two adsorbates can be utilized to tune the binding of one while keeping the other constant under the electric field. This is shown in Figure S17 (Supporting Information), where the presence of a negative electric field enhances the COOH* binding while keeping the CO* binding constant for the Ag 111 adatom and the Ag 111 facet sites. Consistent with the magnitude of the dipole moment, the electric field effect on the Ag 111 adatom is larger than for the Ag 111 facet. Adding the electric field calculations to the volcano plot in Figure 6 (yellow points) shows that the Ag defects allow reduction of $CO_2$ to CO without further reduction of CO. Because the electric double layer thickness is around 3 Å, the electric field effect from just the electrode is in the order of $-0.2\ V\ Å^{-1}$.[9] However, pH and solvated ions can enhance the electric field effect up to $-1.0\ V\ Å^{-1}$,[10] and for the Ag 111 adatom defect only an electric field of about $-0.4\ V\ Å^{-1}$ is required to enable $CO_2$ reduction. The oxygen plasma-treated samples give a highly defective Ag surface, which allows reduction of $CO_2$ at very low overpotentials. Over time, the decrease in surface roughness

  

means that there will be a decrease in the number of defect sites and an increase in terrace-like sites, which will decrease the rate of $CO_2$ reduction and increase the HER.

In summary, we have demonstrated the highly enhanced activity and CO selectivity of Ag catalysts synthesized through facile plasma treatments. Oxygen plasma-treated Ag showed more than 90% Faradaic efficiency towards CO at −0.6 V versus RHE, a significant improvement over metallic Ag which requires more than −0.9 V versus RHE to reduce $CO_2$. TEM and operando EXAFS showed that although reduction of the oxides occurred during the first 30 min of reaction, oxygen remained in the bulk of the catalyst even after 1 h of reaction. However, quasi in situ XPS measurements revealed that the near-surface region of the catalyst is reduced to metallic Ag under reaction conditions within the first 3 min. The mechanism behind the improved reactivity was unraveled by DFT calculations, which indicated that the highly defective surface created by plasma oxidation in the presence of local electric fields can lower the thermodynamic barriers, allowing $CO_2$ reduction to CO at low overpotential. Therefore, our results reveal that a high population of stable defects is critical in creating improved and efficient Ag-based catalysts for $CO_2$ electroreduction.

## Acknowledgements

This work was funded by the Bundesministerium für Bildung und Forschung (BMBF) under grant #03SF0523C—"CO2EKAT", the Cluster of Excellence RESOLV at RUB (EXC 1069) funded by the Deutsche Forschungsgemeinschaft, the European Research Council under grant ERC-OPERANDOCAT (ERC-725915), and the flagship "Climate KIC/EnCO$_2$re" program as part of the Horizon2020 EU funding instrument and the Carlsberg Foundation (grant CF15-0165). Financial support was provided by the US National Science Foundation (NSF-CHEM 1213182). Resources of MRCAT at the Advanced Photon Source operated for the US Department of Energy (DOE) by Argonne National Laboratory (ANL) under Contract No. DE-AC02-06CH11357 were used. MRCAT is funded by the MRCAT member institutions and DOE. User support at beamline 10-ID-B was provided by Joshua Wright. The authors gratefully acknowledge the SAMBA beamline at the Soleil synchrotron facility and user support by Laurent Gautier. C.S.B. and J.C.Y. acknowledge support by NSF-CHE-1534630 and DOE-BES (DE FG02-03ER15476). Dr. Marco Cordeiro is kindly thanked for his technical support during the EDS acquisition. Transmission electron microscopy work was performed at the Center for Functional Nanomaterials, a DOE Office of Science Facility, at Brookhaven National Laboratory under Contract No. DE-SC0012704.

## Conflict of interest

The authors declare no conflict of interest.

**Keywords:** $CO_2$ reduction · electrocatalysis · nanostructures · silver

**How to cite:** *Angew. Chem. Int. Ed.* **2017**, *56*, 11394–11398
*Angew. Chem.* **2017**, *129*, 11552–11556

[1] a) E. V. Kondratenko, G. Mul, J. Baltrusaitis, G. O. Larrazábal, J. Pérez-Ramírez, *Energy Environ. Sci.* **2013**, *6*, 3112–3135; b) D. T. Whipple, P. J. Kenis, *J. Phys. Chem. Lett.* **2010**, *1*, 3451–3458.

[2] a) H. Mistry, R. Reske, Z. Zeng, Z.-J. Zhao, J. Greeley, P. Strasser, B. R. Cuenya, *J. Am. Chem. Soc.* **2014**, *136*, 16473–16476; b) Y. Hori, A. Murata, K. Kikuchi, S. Suzuki, *J. Chem. Soc. Chem. Commun.* **1987**, 728–729.

[3] T. Hatsukade, K. P. Kuhl, E. R. Cave, D. N. Abram, T. F. Jaramillo, *Phys. Chem. Chem. Phys.* **2014**, *16*, 13814–13819.

[4] a) Q. Lu, J. Rosen, F. Jiao, *ChemCatChem* **2015**, *7*, 38–47; b) C. Kim, H. S. Jeon, T. Eom, M. S. Jee, H. Kim, C. M. Friend, B. K. Min, Y. J. Hwang, *J. Am. Chem. Soc.* **2015**, *137*, 13844–13850; c) A. Salehi-Khojin, H.-R. M. Jhong, B. A. Rosen, W. Zhu, S. Ma, P. J. A. Kenis, R. I. Masel, *J. Phys. Chem. C* **2013**, *117*, 1627–1632; d) C. Kim, T. Eom, M. S. Jee, H. Jung, H. Kim, B. K. Min, Y. J. Hwang, *ACS Catal.* **2017**, *7*, 779–785; e) S. Ma, J. Liu, K. Sasaki, S. Lyth, P. Kenis, *Energy Technol.* **2017**, *5*, 861–863; f) S. Ma, Y. Lan, G. M. J. Perez, S. Moniri, P. J. A. Kenis, *ChemSusChem* **2014**, *7*, 866–874.

[5] a) L. Zhang, Z. Wang, N. Mehio, X. Jin, S. Dai, *ChemSusChem* **2016**, *9*, 428–432; b) Y. Yoon, A. S. Hall, Y. Surendranath, *Angew. Chem.* **2016**, *128*, 15508–15512; c) H. Wang, Z. Han, L. Zhang, C. Cui, X. Zhu, X. Liu, J. Han, Q. Ge, *J. $CO_2$ Util.* **2016**, *15*, 41–49; d) Q. Lu, J. Rosen, Y. Zhou, G. S. Hutchings, Y. C. Kimmel, J. G. Chen, F. Jiao, *Nat. Commun.* **2014**, *5*, 1–6.

[6] J. Rosen, G. S. Hutchings, Q. Lu, S. Rivera, Y. Zhou, D. G. Vlachos, F. Jiao, *ACS Catal.* **2015**, *5*, 4293–4299.

[7] a) M. Ma, B. J. Trześniewski, J. Xie, W. A. Smith, *Angew. Chem. Int. Ed.* **2016**, *55*, 9748–9752; *Angew. Chem.* **2016**, *128*, 9900–9904; b) M. S. Jee, H. S. Jeon, C. Kim, H. Lee, J. H. Koh, J. Cho, B. K. Min, Y. J. Hwang, *Appl. Catal. B* **2016**, *180*, 372–378; c) M. S. Jee, H. Kim, H. S. Jeon, K. H. Chae, J. Cho, B. K. Min, Y. J. Hwang, *Catal. Today* **2016**, *288*, 48–53; d) Y.-C. Hsieh, S. D. Senanayake, Y. Zhang, W. Xu, D. E. Polyansky, *ACS Catal.* **2015**, *5*, 5349–5356; e) L. Q. Zhou, C. Ling, M. Jones, H. Jia, *Chem. Commun.* **2015**, *51*, 17704–17707.

[8] a) H. Mistry, A. S. Varela, C. S. Bonifacio, I. Zegkinoglou, I. Sinev, Y.-W. Choi, K. Kisslinger, E. A. Stach, J. C. Yang, P. Strasser, B. Roldan Cuenya, *Nat. Commun.* **2016**, *7*, 12123; b) D. Kim, S. Lee, J. D. Ocon, B. Jeong, J. K. Lee, J. Lee, *Phys. Chem. Chem. Phys.* **2015**, *17*, 824–830; c) A. Eilert, F. Cavalca, F. S. Roberts, J. Osterwalder, C. Liu, M. Favaro, E. J. Crumlin, H. Ogasawara, D. Friebel, L. G. Pettersson, A. Nilsson, *J. Phys. Chem. Lett.* **2017**, *8*, 285–290; d) Y. Chen, M. W. Kanan, *J. Am. Chem. Soc.* **2012**, *134*, 1986–1989; e) A. Dutta, A. Kuzume, M. Rahaman, S. Vesztergom, P. Broekmann, *ACS Catal.* **2015**, *5*, 7498–7502; f) C. W. Li, M. W. Kanan, *J. Am. Chem. Soc.* **2012**, *134*, 7231–7234; g) Y. Chen, C. W. Li, M. W. Kanan, *J. Am. Chem. Soc.* **2012**, *134*, 19969–19972.

[9] J. Rossmeisl, J. K. Nørskov, C. D. Taylor, M. J. Janik, M. Neurock, *J. Phys. Chem. B* **2006**, *110*, 21833–21839.

[10] L. D. Chen, M. Urushihara, K. Chan, J. K. Nørskov, *ACS Catal.* **2016**, *6*, 7133–7139.

Manuscript received: May 4, 2017
Revised manuscript received: June 13, 2017
Accepted manuscript online: July 14, 2017
Version of record online: August 10, 2017

  